Supplementary Material

1 XCT acquisition and workflow

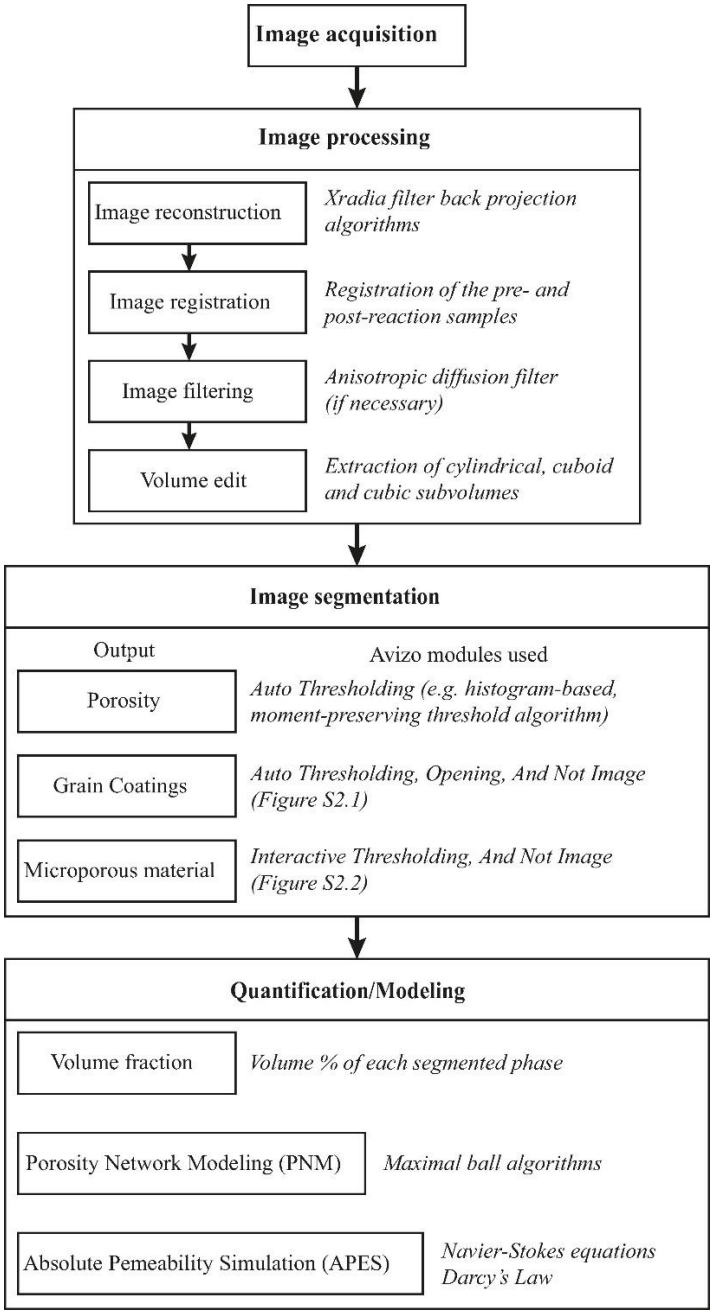

Figure S1.1: XCT processing workflow devised for pore phase, grain coating and microporous material analysis, and porosity and permeability modeling.

Sample	Voltage (kV)	Current (mA)	Exposure time (s)	Voxel size (µm)	Sample volume	Data size (voxel)	Data size (mm)
S1	80	125	2	3.8	full sample	1416 x 1458 x 1687	5.4 x 5.5 x 6.4
	-	-	-	3.8	cylindrical	945 x 943 x 930	3.6 x3.6 x 3.5
S2	80	125	2	3.8	full sample	1364 x 1383 x1820	5.2 x 5.3 x 6.9
	-	-	-	3.8	cylindrical	945 x 943 x 1130	3.6 x 3.6 x 4.3
S3	80	125	2	3.8	full sample	1379 x 1377 x 1757	5.2 x 5.5 x 6.7
	-			3.8	cylindrical	944 x 943 x 884	3.6 x 3.6 x 3.4
S4	80	125	2	3.8	full sample	1351x1346x1757	5.1 x 5.1 x 6.7
	-	-	-	3.8	cylindrical	942 x 939 x 1023	3.6 x 3.6 x 3.9
S5	80	125	2	3.8	full sample	1335 x 1419 x 1818	5.1 x 5.4 x 6.9
	-	-	-	3.8	cylindrical	944 x 943 x 1037	3.6 x 3.6 x 3.9
S1-S5	-	-	-	3.8	cubic	500 x 500 x 500	1.9 x1.9x 1.9
S6A	80	120	1	5.6	full sample	768 x 742 x 4000	4.3 x 4.2 x 22.4
	-	-	-	5.6	cuboid	333 x 334 x 3548	1.9 x 1.9 x 19.9
S6B	80	120	1	1.7	full sample	1880 x 1880 x 3560	3.2 x 3.2 x 6.1
	-	-	-	1.7	cuboid	1104 x 1159 x 2918	1.9 x 2 x 5
S6C1-C3	-	-	-	1.7	cubic	500 x 500 x 500	0.9 x 0.9 x 0.9

Table S1.1: XCT acquisition characteristics of the raw data (full sample) and size of the analyzed subvolumes.

Raw XCT data are available online at http://doi.org/10.15128/r30v838056z (S1, S2, S5), http://doi.org/10.15128/r32514nk484 (S6A), and http://doi.org/10.15128/r3bc386j205 (S6B).

2 Segmentation process

2.1 Grain coating segmentation process

The bright phase (both grain coating and pore filling) was segmented using a histogram-based, moment-preserving threshold algorithm [Tsai, 1985]. The user-defined low and high threshold greyscale values used by the algorithm to determine the placement of the phase interface are presented in Table S2.1. Subsequently, the opening Avizo module was applied to perform a 3D opening of the segmented binary image, using a spherical structuring element, discarding small objects and keeping the largest ones with similar shape in the original and the final image. Then a logical difference between the binary image of the overall bright phase and the pore filling bright phase was applied to acquire the grain coatings (Figure S2.1).

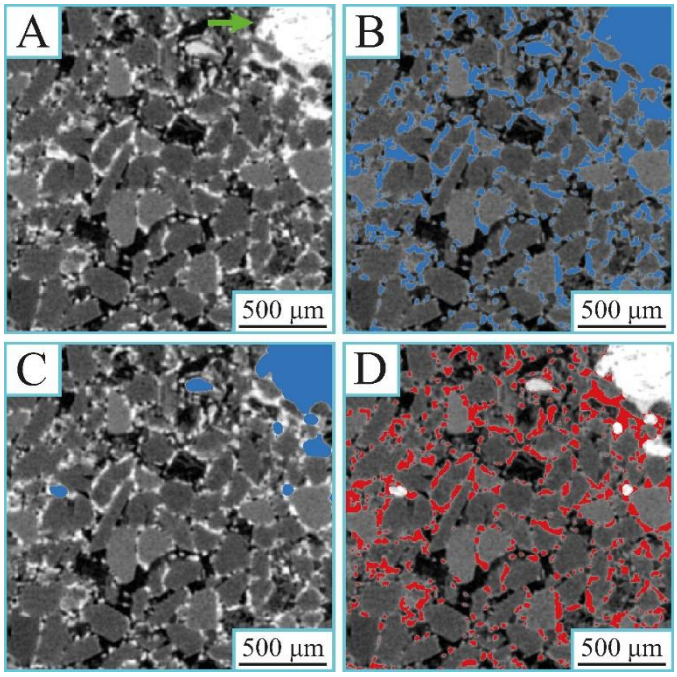

Figure S2.1: Grain coating segmentation process. (A) 2D tomogram of the Cook Formation (sample S5) at a resolution of 3.8 µm/voxel. (B) Selection of the bright phase, including grain coating and pore filling (green arrow) phases. (C) Selection of the pore filling bright phase. (D) Selection of the bright phase fringing the host grains (e.g., grain coatings).

Sample	**T (°C)**	**Bright phase**	
		Pre-exp	Post-exp
S1 (cylinder)	100	6700-11800	6900-12000
S2 (cylinder)	150	9000-15200	7500-14500
S3 (cylinder)	200	6700-14500	6500-14600
S4 (cylinder)	225	6400-14500	8900-15000
S5 (cylinder)	250	3700-8000	10800-17800
S1 (cube)	100	6600-11500	6700-11600
S2 (cube)	150	9800-13600	8300-12450
S3 (cube)	200	7600-11200	7400-11000
S4 (cube)	225	7300-11000	9800-12500
S5 (cube)	250	4000-6600	11300-16000
S6A (5.57 µm/voxel)	0	17000-24500	
S6A (5.57 µm/voxel)	100	17000-23600	
S6A (5.57 µm/voxel)	150	17000-24200	
S6A (5.57 µm/voxel)	200	16500-23000	
S6A (5.57 µm/voxel)	250	13300-17000	
S6B (1.7 µm/voxel)	0	12000-20300	
S6B (1.7 µm/voxel)	100	12000-20300	
S6B (1.7 µm/voxel)	150	12000-20300	
S6B (1.7 µm/voxel)	200	11000-15300	
S6B (1.7 µm/voxel)	250	10800-15200	

Table S2.1: User-defined thresholding greyscale range employed by the moment preserving algorithm for the determination of the bright phase.

2.2 Porosity and microporous material segmentation process

The imaged pore phase was segmented using a histogram-based, moment-preserving threshold algorithm [Tsai, 1985]. The user-defined low and high threshold greyscale values used by the algorithm to determine the placement of the phase interface are presented in Table S2.2. Subsequently, imaged porosity combined with microporous regions were segmented using an interactive (or watershed) threshold algorithm (Table S2.3). The microporous material volume was acquired by applying a logical difference between the initial porosity binary image and the result of the last segmentation (Figure S2.2).

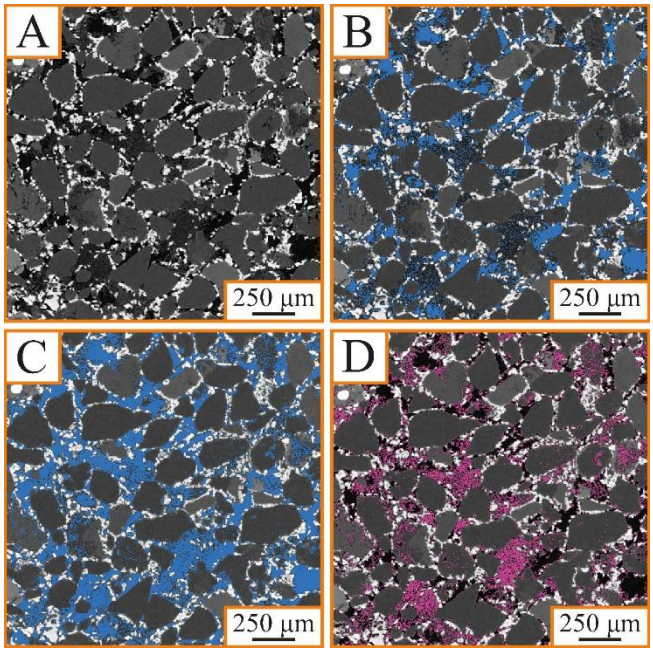

Figure S2.2: Porosity and microporous material segmentation process. (A) 2D tomogram of the Cook Formation (sample S6B) at a resolution of 1.7 µm/voxel. (B) Selection of the imaged porosity. (C) Segmentation of the pore space combined with microporous regions, such as pore filling clays and fractures within the framework grains. (D) Selection of the microporous volume.

Sample	T (°C)	Porosity	
		Pre-exp	Post-exp
S1 (cylinder)	100	3400-6700	4300-6750
S2 (cylinder)	150	6800-9000	5300-7800
S3 (cylinder)	200	4800-6900	4800-6900
S4 (cylinder)	225	4200-6600	7000-9000
S5 (cylinder)	250	2800-3700	8000-10600
S1 (cube)	100	3400-6700	4400-6750
S2 (cube)	150	7500-9000	6100-7700
S3 (cube)	200	5000-7400	5000-7400
S4 (cube)	225	4400-6700	7000-9000
S5 (cube)	250	2650-3850	7000-10750
S6A (5.57 µm/voxel)	0	7000-15000	
S6A (5.57 µm/voxel)	100	8500-15000	
S6A (5.57 µm/voxel)	150	7000-15000	
S6A (5.57 µm/voxel)	200	7000-14800	
S6A (5.57 µm/voxel)	250	11200-12200	
S6B (1.7 µm/voxel)	0	8000-12500	
S6B (1.7 µm/voxel)	100	8000-12500	
S6B (1.7 µm/voxel)	150	8000-12500	
S6B (1.7 µm/voxel)	200	8000-11200	
S6B (1.7 µm/voxel)	250	8000-11200	

Table S2.2: User-defined thresholding greyscale range employed by the moment preserving algorithm for the determination of the porosity phase.

Sample	T (°C)	Porosity + microporous volume
S6B (1.7 µm/voxel)	0	9900-12300
S6B (1.7 µm/voxel)	100	9900-12300
S6B (1.7 µm/voxel)	150	9900-12300
S6B (1.7 µm/voxel)	200	9900-11050
S6B (1.7 µm/voxel)	250	9900-11050

Table S2.3: User-defined thresholding greyscale range employed by the moment preserving algorithm for the determination of the combination of the porosity and microporous material phases.

3 Marker extent parameter

The separate Avizo module was used to separate the connected pore network into a set of connected and labeled pores. The degree of separation, important for the Pore Network Modelling (PNM), is dictated by the marker extent parameter. This is a contrast factor controlling the size of seeds marking objects to be separated. The smaller this parameter is the more separated the main pore network will be, and smaller individual pores will be generated and identified. Contrarily, increasing this value can merge some markers and therefore decrease the number of separated pores. 2D-3D visualization was performed for each rock individually (pre- and post-reaction) to reliably determine the detachment of the pore structures in order to avoid under- or over-separation (Figure S3.1).

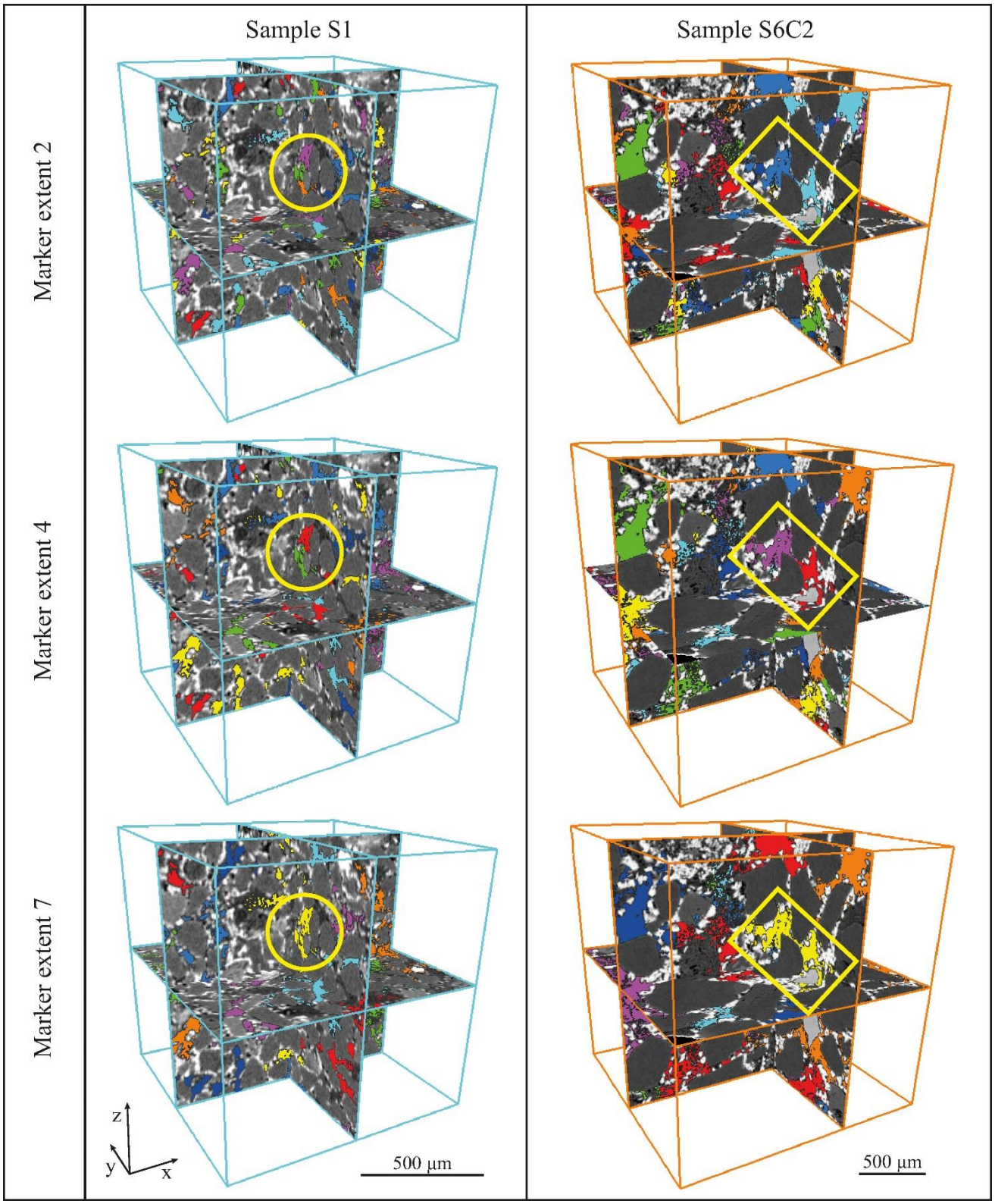

Figure S3.1: 2D-3D examination of samples S1 and S6C2 to determine the marker extent parameter. Regardless of the difference in the resolution of the two samples, a marker extent value of seven is the

most valid. Note the degree of separation (examples outlined in yellow) with increasing the marker extent value for each sample. The value of 2 and 4 over-separates the pore network.

4 Scanning resolution effect

The effect of the scanning resolution on the quantification of the phases of interest between the samples from both experimental suites before hydrothermal treatment was evaluated (Figure S4.1). Namely, the cubic subvolume of sample S4 was cropped to match the volume of sample S6C2. Subsequently, the resample Avizo module with the maximum filter, that preserves tiny dark features on a bright background, was used to downsample (e.g., shrink the dimensions of the regular grid while recalculating the data according to it) sample S6C2 (1.7 μm/voxel) to match the resolution of sample S4 (3.8 μm/voxel). The volume fraction Avizo module was then used to quantify the pore and grain coating material phase of each sample to ascertain the resolution effect.

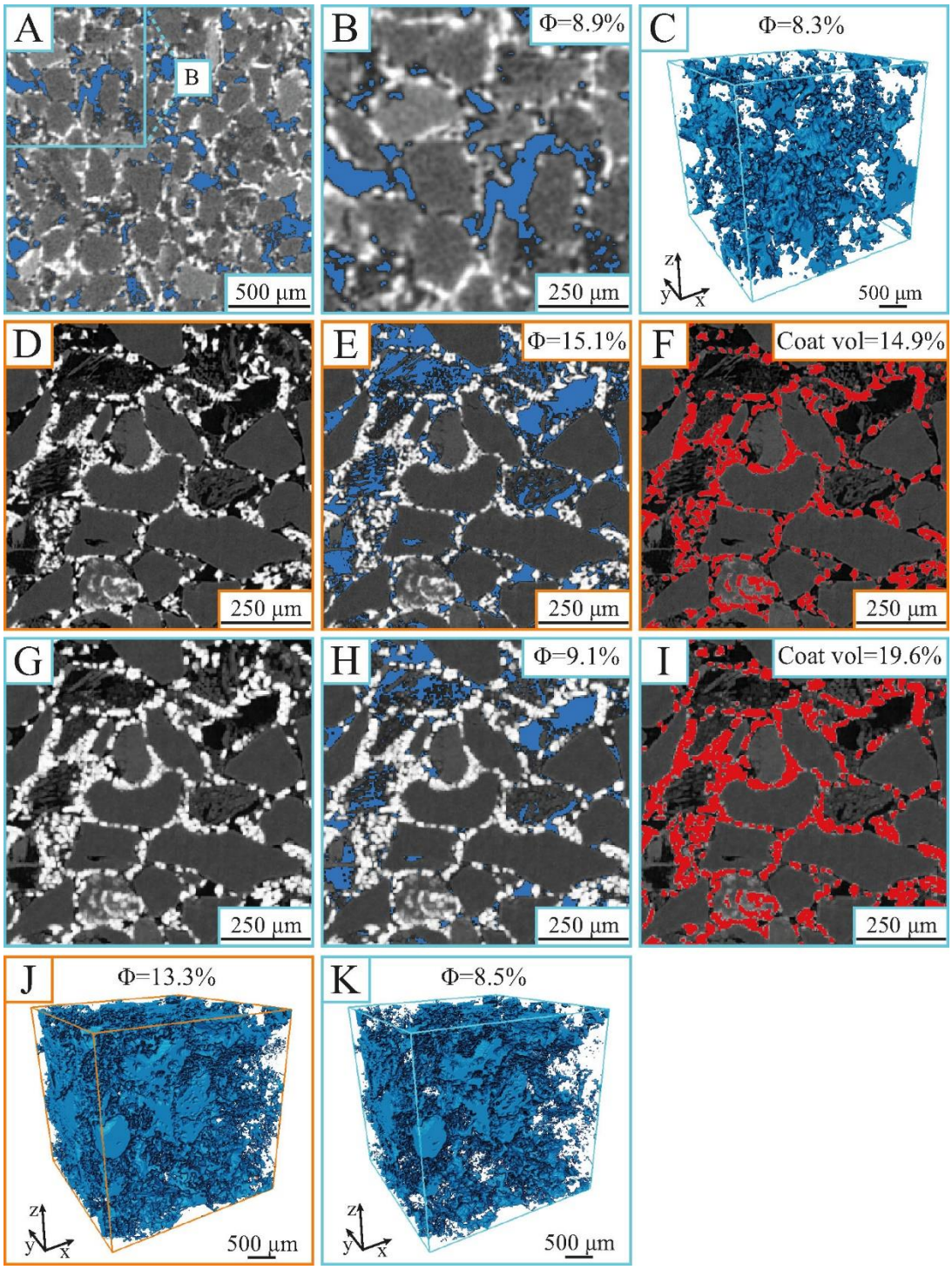

Figure S4.1: Comparison between the lower resolution samples S1-S5 belonging to the first set of experiments with the higher resolution sample S6C2 of the second set of experiments. (A) Greyscale slice of sample S4 with associated porosity phase. (B) Cropped 2D slice matching the dimensions of sample SC62. (C) 3D render of sample S4 after being cropped. D) Greyscale image of sample S6C2 and associated pore (E) and grain coatings (F) phase. (G) Downsampled greyscale slice of sample S6C2

with associated porosity (H) and grain coating volume (I). 3D Porosity render before (J) and after (K) the downsampling.

5 Porosity modeling and permeability simulations

The XCT-captured 3D geometry of the pore phase of the hydrothermally treated samples was further used to construct pore network models and computationally simulate fluid flow to determine permeability. Namely, a topologically equivalent network of the pores and throats from the 3D XCT images was extracted based on the maximum ball concept [*Dong et al.*, 2007; *D Silin and Patzek*, 2006; *D B Silin et al.*, 2003], providing quantitative information regarding the coordination number (e.g., number of throats connected to a given pore), radius, area, and volume of each pore as well as the radius and length of each throat. Single-phase flow simulations of the interconnected porosity phase were computed via the implementation of the finite volume method [*Harlow and Welch*, 1965] and Stokes equations. The Stokes equations are given by:

$$\nabla \cdot u = 0 \quad (2)$$

$$\mu \nabla^2 u - \nabla p = 0 \quad (3)$$

$$u = 0 \text{ on grains} \quad (4)$$

Where p is the pressure (Pa), $\mu = 1x10^{-3}$ Pa.s is the viscosity of water, u is the fluid velocity vector ($m.s^{-1}$), and ∇ indicates the gradient differential operator.

Permeability (k) is obtained by the application of Darcy's Law:

$$k = -Q \frac{\mu}{\Delta P} \frac{L}{A} \quad (4)$$

Where ΔP is the gradient of pressure applied to the boundary (input pressure - output pressure), A is the cross-sectional area (m^2), and L is the length of the computational domain.

6 References

Dong, H., M. Touati, and M. J. Blunt (2007), Pore Network Modeling: Analysis of Pore Size Distribution of Arabian Core Samples, in *SPE Middle East Oil and Gas Show and Conference*, edited, p. 5, Society of Petroleum Engineers, Manama, Bahrain, doi:10.2118/105156-MS.

Harlow, F. H., and J. E. Welch (1965), Numerical Calculation of Time-Dependent Viscous Incompressible Flow of Fluid with Free Surface, *The Physics of Fluids*, *8*(12), 2182-2189, doi:10.1063/1.1761178.

Silin, D., and T. Patzek (2006), Pore space morphology analysis using maximal inscribed spheres, *Physica A: Statistical Mechanics and its Applications*, *371*(2), 336-360, doi:10.1016/j.physa.2006.04.048.

Silin, D. B., G. Jin, and T. W. Patzek (2003), Robust determination of pore space morphology in sedimentary rocks, paper presented at Annual Technical Conference and Exhibition.